Ocean Radar Backscatter Relationship with Near-Surface Winds: A Case Study during FASINEX

F. LI,* W. LARGE,** W. SHAW,+ E. J. WALSH,‡,@ AND K. DAVIDSON+

*Jet Propulsion Laboratory, California Institute of Technology, Pasadena, California
**National Center for Atmospheric Research, Boulder, Colorado
+Naval Postgraduate School, Monterey, California
‡Goddard Space Flight Center, National Aeronautics and Space Administration, Greenbelt, Maryland

(Manuscript received 20 November 1987, in final form 29 August 1988)

ABSTRACT

A case study of the ocean radar backscatter dependence on near-surface wind and wind stress is presented using the data obtained on 18 February 1986 during the Frontal Air–Sea Interaction Experiment. Our interest in this case stems from the particular wind–wave conditions and their variations across a sharp sea surface temperature front. These are described. Most importantly, the small change in wind speed across the front cannot account for the large change in wind stress implying significant changes in the drag coefficient and surface roughness length. When compared with previous results, the corresponding changes in radar backscatter cross-section at 50° and 20° angles of incidence were consistent with the observed variations in wind stress, but inconsistent with both the mean wind and the equivalent neutral wind. Although not definitive, the results strengthen the hypothesis that radar backscatter is closely correlated to wind stress, and therefore, could be used for remote sensing of the wind stress itself over the global oceans.

1. Introduction

Over the past 15 years, numerous airborne and spaceborne scatterometer experiments have demonstrated that the radar backscatter cross section, σ_0, of the ocean is related to the near-surface wind velocity (Jones et al. 1977; Moore and Fung 1979; Schroeder et al. 1982). Presently, two spaceborne scatterometers are being constructed for launch in the early 1990s for global ocean wind measurements (Li et al. 1984). However, despite all these studies, there remain substantial uncertainties in the relationship between σ_0 and the wind. A key unanswered question is: what wind-related variable is the most appropriate to correlate with σ_0. Early attempts simply used measurements of mean wind speed U and direction (Moore and Fung 1979). Other candidates that have since been explored are the equivalent neutral stability wind, U_N (Schroeder et al. 1982) and the friction velocity, u^* (Liu and Large 1981).

The friction velocity is the fundamental velocity scale in the atmospheric surface layer, where it determines the structure of the turbulence (Monin and Yaglom 1965). It is defined by

$$u^{*2} = \rho^{-1}|\vec{\tau}|$$

where ρ is air density and $\vec{\tau}$ is the surface wind stress. Since variations in ρ are small, a measurement of u^* gives the magnitude of the wind stress. The near-surface wind profile depends also on the vertical stratification, which is quantified by the stability parameter $\zeta = z/L$:

$$U(z) = \frac{U^*}{\kappa}\left[\ln\left(\frac{z + z_0}{z_0}\right) - \psi(\zeta)\right], \qquad (1)$$

where z is height, L is the Monin-Obukhov length, κ is von Kármán's constant (0.4), and z_0 is the surface roughness length. Large and Pond (1982) give a more detailed development and show a method for computing ζ, $\psi(\zeta)$, and L from mean wind, temperature and humidity measurements.

The empirical relation $\psi(\zeta)$ has been formulated so that as stratification changes, resulting modifications in $U(z)$ are accounted for by $\psi(\zeta)$, allowing both u^* and z_0 to remain unchanged. A convenient wind parameter that utilizes this property is the equivalent neutral wind,

$$U_N(z) = \frac{u^*}{\kappa}\ln\left(\frac{z + z_0}{z_0}\right). \qquad (2)$$

The relationships between these wind parameters define the drag coefficient, C_D and its equivalent neutral value, C_N,

$$u^{*2} \equiv C_D(z, \zeta)U^2(z) \equiv C_N(z)U_N^2(z). \qquad (3)$$

@ Presently on assignment at the NOAA/ERL Wave Propagation Laboratory, Boulder, CO.
Corresponding author address: Dr. Fuk K. Li, Jet Propulsion Laboratory, California Institute of Technology, 4800 Oak Grove Drive, Pasadena, CA 91109

For many purposes it is u^* that needs to be derived from σ_0 measurements. The surface stress, or momentum flux from the atmosphere to the ocean is the principle driver of ocean circulation. Also, the sensible and latent (moisture) heat fluxes are directly proportional to u^*. It would be advantageous to relate σ_0 directly to u^*, because it would eliminate the uncertainties in the derived fluxes associated with the drag coefficient, which enter if a σ_0 to U_N relationship is used. However, routine, direct measurements of u^* have become common only recently. Most efforts, therefore, have attempted to relate σ_0 to $U_N(19.5\text{ m})$, which is computed from $U(z)$ measured from surface buoys and ships, and from low flying aircraft. An example of the latter relationship is the SASS-1 model (Schroeder et al. 1982) that was derived using Seasat satellite scatterometer (SASS) and aircraft scatterometer data. For $z \gg z_0$, (2) and (3) become

$$u^* = \frac{\kappa U_N(z)}{\ln(z/z_0)} = (C_N(z))^{1/2} U_N(z), \qquad (4)$$

so the SASS-1 model and a σ_0 to u^* formulation cannot both hold whenever z_0, and hence $C_N(z)$, vary from their norms. Transforming $U(z)$ measurements to $U_N(z)$ accounts for stratification, making σ_0 to $U_N(z)$ formulations preferable to σ_0 to $U(z)$ relations (see arguments in Halberstam 1980).

Existing experimental results cannot settle these issues. The only extensive comparison of u^* and U_N correlations with σ_0 was reported by Liu and Large (1981). With a set of u^* measurements derived from direct observations, not inferred from the mean wind, they demonstrated that the correlation between σ_0 and u^* was as good as that between σ_0 and U_N. They suggest that a study in more extreme conditions, in which u^* and U_N variations were clearly different, is required to shed light on this problem. We note that there are suggestions that other geophysical parameters, besides near surface winds, are important in understanding ocean backscatter. Examples of these parameters include surface waves (Keller et al. 1986), and sea surface temperature, SST (Woiceshyn et al. 1986). However, some of these effects may not be independent of the wind parameters, since z_0, and hence u^* for a given $U_N(z)$, can depend on surface waves (Huang et al. 1986) and ζ depends on the sea–air temperature difference and the wind.

We have taken a significant step by collecting and analyzing a limited data set during the Frontal Air–Sea Interaction Experiment (FASINEX). Stage and Weller (1985) provide an overview of the experiment. The data of interest here consist of σ_0 measured at 14 GHz from an aircraft, wind stress and other ocean/atmosphere variables measured from aircraft and ships. The purpose of this paper is to present the results obtained on 18 February 1986, when the u^* and U_N variations across the SST front were observed to be markedly different. The results obtained were used as a case study of σ_0 dependence on wind, wave and atmospheric stratification. Although the results are not definitive, they strongly suggest that σ_0 correlates much better with u^* than with U or U_N.

2. Experiment

FASINEX was designed to evaluate the air–sea interaction processes around an oceanic surface temperature front in the subtropical convergence zone of the western North Atlantic Ocean. A mooring array with five surface meteorological buoys was deployed from January to June 1986 near 27°N, 69.5°W, about 500 km southwest of Bermuda. During the intensive experiment period, the research vessels *Endeavor* and *Oceanus* and up to six aircraft performed oceanographic and meteorological measurements at various oceanic fronts. The aircraft were the NOAA P-3D, NCAR Electra, NRL P-3A, NASA Ames C-130B, NASA Wallops P-3, and NASA Electra. On 18 February 1986, the research aircraft flew in formation across and along a sea surface temperature front to make more detailed and area-extensive measurements. Figure 1a shows a schematic diagram of the SST front position, the ship locations and the aircraft flight pattern. Figure 1b is a schematic diagram of the relative flight positions of the research aircraft during their formation flight. There were many measurements performed from these platforms and the following are the instruments and measurements of interest to this case study.

A. The 14 GHz radar scatterometer on NASA C130B

The Airborne Microwave Scatterometer (AMSCAT) operated from the NASA Ames C130B. It sent out

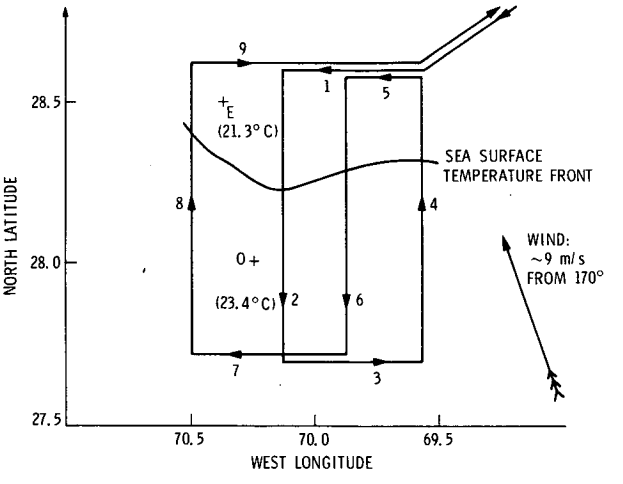

FIG. 1a. A schematic diagram showing the flight pattern of the airplanes on 18 Feb 1986, the locations of the research ships and approximate locations of the sea surface front as measured by the airplanes. The data from flight lines 2, 4 and 6 are discussed in this paper.

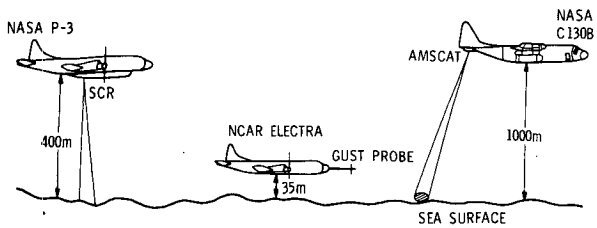

FIG. 1b. A schematic diagram showing the formation flights of the three airplanes discussed in this paper.

short, gated CW pulses at 14.6 GHz through a parabolic antenna with a beamwidth of ~3 degrees. Both horizontal and vertical polarization measurements were obtained. During a typical flight line the antenna was fixed at a chosen elevation angle (incidence angle on ocean surface). The antenna was then programmed to step 10° in azimuth every 4 seconds. Since the scan-rate of the antenna gimbal system was ~10°/sec, the azimuthal angles were nearly constant 3 out of every 4 seconds. Due to the potential blockage of the antenna pattern by the fuselage of the C130B, azimuth scans were stopped ±15° relative to the forward center line of the airplane. The scan pattern was then reversed and the azimuth scans continued. Before and immediately after a flight line, internal calibration of AMSCAT was performed, which allows the ocean backscatter signals be reduced into relatively calibrated $\sigma_0 s$. Based on the number of independent echoes averaged, the uncertainties of the geometric parameters, and the calibration signal accuracy, we estimate that the relative σ_0 accuracy was ~0.3 to 0.5 dB. We note that the noise level of one of the two amplifier–detector systems was found to drift gradually during FASINEX, but most of the data presented in this paper were collected by the system with no drift, and therefore the corrections do not affect our conclusion.

Figure 2 shows the σ_0 obtained during flight line 2 (see Fig. 1a). The data were collected using vertical polarization and a commanded incidence angle of 50°. The σ_0 observed were plotted as a function of the latitude of the aircraft along with the antenna azimuth angle relative to due North. We note that the crossing was basically along a constant longitude and the use of latitude in Fig. 2 allows us to align the data from different aircraft. Due to the attitude variations of the C130B, the actual incidence angles on the ocean surface differed slightly from 50°. Using the neutral stability wind observed by the ships (see below), and the SASS-I model, we computed the adjustments for incidence angle variations. We note that the typical adjustment was ≤0.1 dB and does not affect our conclusion.

A PRT-5 on the C130B was used to obtain sea surface temperature measurements. These temperature measurements (Fig. 2) have been adjusted to conform with the sea surface temperature measurements from the ships. We did not attempt to remove cloud contaminations on these PRT-5 results. One can easily see a sharp sea surface temperature front with a 2°C temperature change in less than ~10 km. The maximum gradient is ~0.5°C in 1 km.

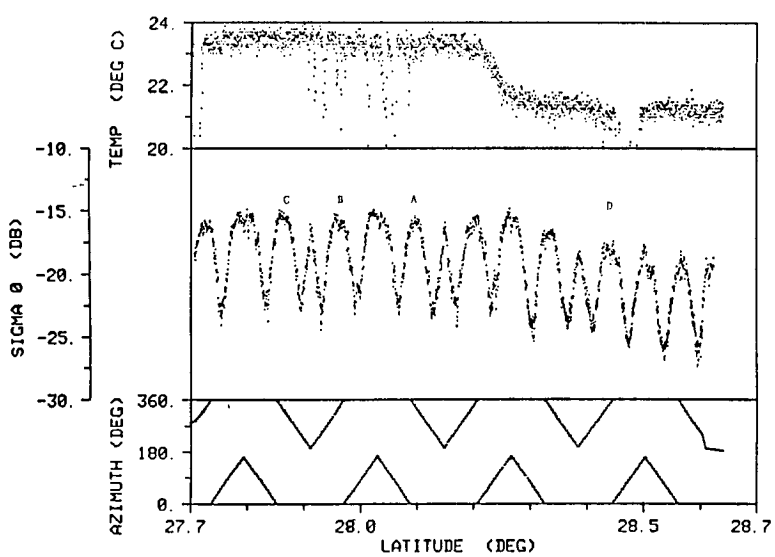

FIG. 2. The radar backscatter cross section (σ_0) is plotted vs time for flight line 2. Also plotted are: a. the sea surface temperature (SST) measured by the PRT-5 on the C130 that had been adjusted to conform to the measured SST from the two ships; and c. the azimuth angle of σ_0 observations relative to due North. The periodic modulation of σ_0 correspond to the well-known azimuthal σ_0 modulations as the antenna was scanned in a near complete circle. The σ_0 data were obtained with vertical polarization, at 50° incidence angle.

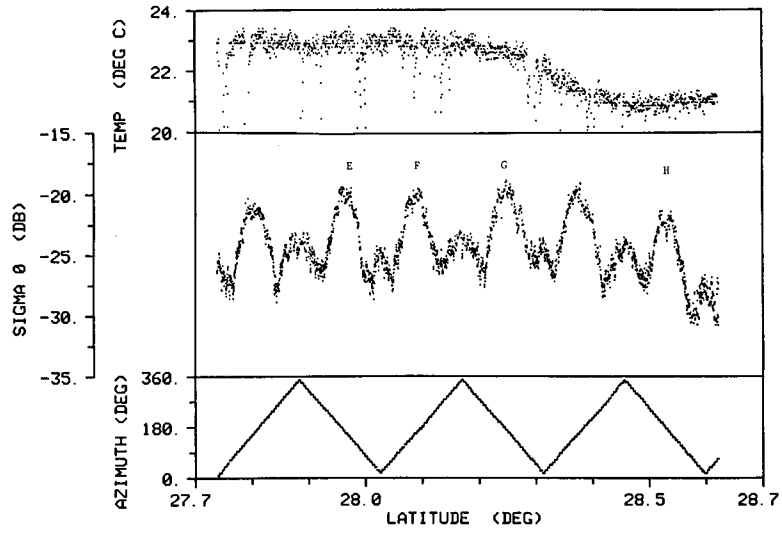

FIG. 3. As in Fig. 2 except the data are for flight line 4 with horizontal polarization, at 50° incidence angle.

An obvious feature of Fig. 2 is the change of σ_0 across the front. The average σ_0 values at the downwind maxima were obtained by fitting the σ_0 data within ±12 seconds of the maxima to a parabolic function. We picked the downwind maxima rather than the upwind for this flight line because the antenna gimbal was programmed to reverse its scan before actually crossing over the upwind azimuth direction. It is also interesting to note that the σ_0 change was apparently gradual and extended north of the SST front (i.e., the σ_0 change occurred on the downwind side of the front). In section 3, this change in σ_0 is compared with the other observations described below.

We also observed similar σ_0 variations across the front on flight line 4 (Fig. 1a). For this flight line, the σ_0 data were obtained using horizontal polarization at 50° incidence angle. The results are plotted on Fig. 3. From the observed SST, the location of the sea surface temperature front was further north compared to that observed in flight line 2 and was not as sharp. Thus, we may not have observed a complete transition of the σ_0 towards the cold side of the front as we did on flight line 2. However, the results still clearly indicate a gradual but significant decrease of σ_0 towards the cold side.

We have also examined the σ_0 results in flight lines 6 and 8, which were obtained at incidence angle of ~20°. For flight line 8, the sea surface temperature front occurred even further north than line 4 (Fig. 1a) and the data were not used to study the above phenomenon. The data in flight line 6, obtained using horizontal polarization, were processed in a manner similar to flight lines 2 and 4 above (Fig. 4). However, due to the relatively larger variations of σ_0 with incidence angle for data obtained near 20° (see the SASS-1 model), the adjustments required to compensate for the incidence angle variations were substantially larger. Again, we fitted the adjusted data within ±12 seconds of the maxima to a parabolic function and the fitted peak σ_0 values were measured. A smaller, but statistically significant, change of σ_0 across the front was observed (see Table 2c and section 3 below).

b. NCAR electra wind stress measurements

The aircraft-derived wind measurements were obtained by the NCAR Electra. The Electra used a gust probe–inertial navigation system to obtain measurements of the mean and fluctuating vector wind. This system is described in detail by Lenschow and Spyers-Duran (1987). The data were acquired at a sampling rate of 20 Hz and the aircraft flight speed was approximately 100 m s^{-1}, yielding a Nyquist wavenumber of 0.1 cyc/m. During flight lines 2, 4 and 6, the average altitude of the Electra was 40 m.

Analysis of the FASINEX Electra data raises questions which are still unresolved regarding averaging intervals for the Reynolds flux and variance calculations. The primary goal of the measurement program was to investigate the structure of the atmospheric boundary layer in the presence of the well-defined inhomogeneity of a sea surface temperature front. However, under these conditions the choice of averaging distances for Reynolds flux and variance calculations becomes an ill-defined balance between minimizing the effect of spatial inhomogeneity of the second-moment field on any one estimate and maximizing the statistical significance of that estimate.

We have chosen a filtering and averaging scheme based upon well-known characteristics of the vertical velocity spectrum. In the surface layer of the atmosphere, the peak of this spectrum occurs at a wavelength roughly equal to the measurement height, and the

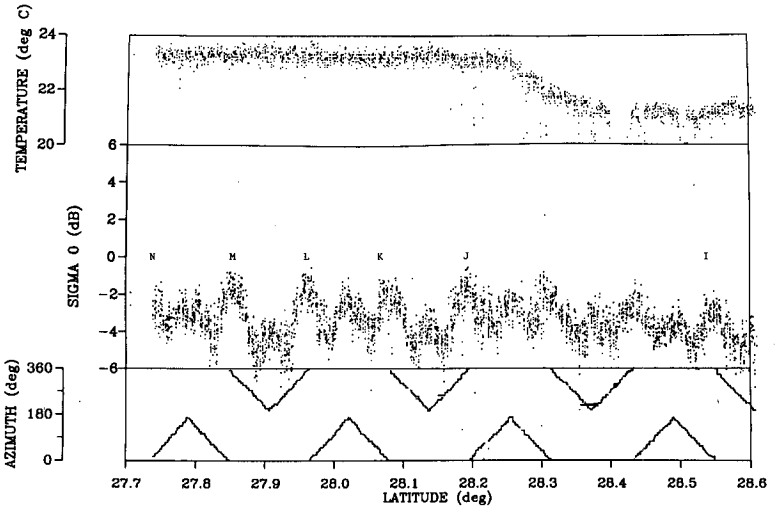

FIG. 4. As in Fig. 2 except the data are for flight line 6 with horizontal polarization, at 20° incidence angle.

spectral density decreases substantially in magnitude toward both longer and shorter wavelengths (e.g., Kaimal et al. 1972). Therefore, at wavelengths several orders of magnitude longer than the peak, the vertical velocity should make a substantially smaller contribution to the vertical fluxes, including stress.

We have used a 10 km running mean subtraction filter to remove low frequencies from the data because of its ease of implementation and its well-defined transfer function. We have also used a 10 km averaging interval for stress calculation to minimize effects of spatial variability of the stress field on each estimate. One may use Wyngaard's (1973) arguments (with Taylor's hypothesis) to obtain an estimate of the uncertainty of stress obtained in the above fashion. The fractional error, a, in a momentum flux calculation is given by:

$$a^2 = 100z/D \qquad (5)$$

where z is the measurement height and D is measurement distance along a flight path. Substituting for z = 45 m and D = 10 000 m yield a = 0.67. For calculation of u^* consideration of propagation of error gives an uncertainty of roughly 30%. [More recent work (Wyngaard 1985; Lenschow and Stankov 1986) paints a somewhat gloomier picture of the prospects for these direct Reynolds stress measurements in the atmospheric boundary layer.]

The variance and covariance (fluxes) are computed by integrating the spectral and cospectral density. These data have been generated using a standard fast Fourier transform (FFT) routine on data blocks of 2048 points. These blocks correspond identically to those from which the basic stress estimates have been calculated by cross-multiplying the filtered time series and then averaging. The transform blocks overlap slightly to provide for a 10 km (2000 point) spatial separation between spectral estimates.

The values of u^* derived from flight lines 2, 4 and 6 are plotted in Fig. 5. The variation in u^* across the front is evident, but it is not highly significant, because of the large error (5). Additional ship data are needed. The corresponding variations in U and U_N are smaller and will be discussed below.

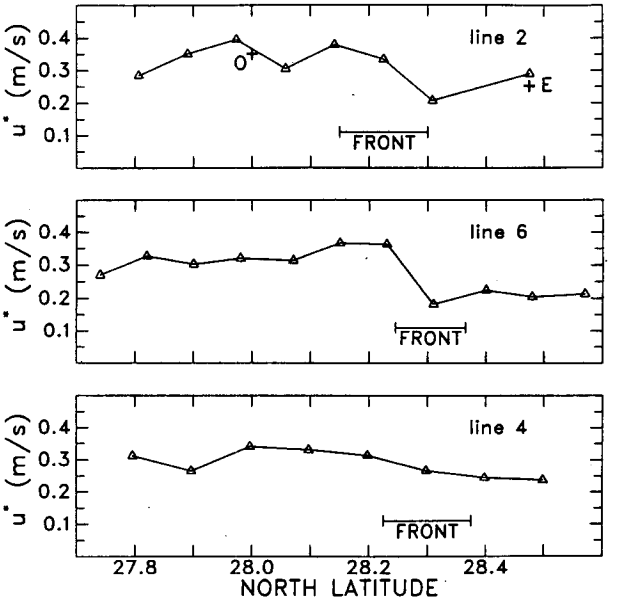

FIG. 5. Time series of Electra u^* values from flight lines 2, 4 and 6, ordered so that west to east runs top to bottom. Also shown are the locations of the frontal regions and the corresponding u^* values from *Endeavor* (E) and Oceanus (O) during flight line 2.

c. Ship data

The wind measurements from the ships involve very different instrumentation and data processing techniques from those of the Electra and their errors are of a very different nature. For wind stress (u^*) measurements, the inertial dissipation technique was employed on the ships. This method is based on a consideration of the turbulent kinetic energy budget, assumes steady horizontally homogeneous flow, and relies on empirical constants such as κ and K' (the one-dimensional Kolmogoroff). The primary measurement is the spectral density of the horizontal wind at high frequencies in the inertial subrange. The advantage is that it is possible to obtain stable 20 minute estimates of u^* even from an unstable moving platform, such as a ship, because these frequencies are higher than those of the ship's motion, and only the mean wind relative to the anemometer needs to be determined. A comparison of the two techniques shows that the inertial dissipation method is viable, with systematic and random uncertainties in u^* of 3% and 10%, respectively (Large and Pond 1981). However, there is always a possibility that at any particular time the meteorological conditions are such that not all the necessary assumptions are valid.

The *Endeavor* wind speeds and stresses are derived from Gill propeller anemometer data, as described, tested, and evaluated in Large and Businger (1988). The design target was 10% accuracy in u^*, and no evidence to the contrary was found. The *Oceanus* stress estimates were based on hot film anemometry, while fast response cup anemometers provided the mean wind speed. A conservative estimate of the uncertainty in the ship u^* values is 15%. Supplementary data such as ship speed and heading, atmospheric temperature and humidity, and SST were obtained on both ships' SAIL system and from the Naval Postgraduate School's instrument suite. The latter system, including the hot film data processing, are described in Guest and Davidson (1987).

The *Endeavor* and *Oceanus* estimates of u^* most nearly coinciding with the aircraft overflights during flight line 2 are plotted in Fig. 5. They are in excellent agreement with the Electra results. Shipboard mean measurements of wind speed, air–sea temperature difference and air–sea humidity difference were used to estimate the atmospheric stability parameter, which in turn was used to shift both aircraft and ship winds to 10.0 and 19.5 m height and to neutral stratification. On the warm side, ζ was near zero, indicating neutral conditions where U and U_N are equal. On the cold side, the lower SST led to quite stable stratification with $\zeta \sim 0.046$ at $z = 10$ m. Therefore, the change in U_N across the front was greater than the change in U.

d. Surface wave measurements

Another dataset of interest is the surface wave height data obtained by the Surface Contour Radar (SCR) that operated on the NASA Wallops P-3. The SCR is a 36 GHz computer-controlled airborne radar (Kenny et al. 1979), which routinely produces ocean directional wave spectra. Figure 6 shows the nominal measurement geometry and the horizontal resolutions in terms of the aircraft altitude. An oscillating mirror scans a 1.42° half-power width pencil-beam laterally to measure the elevations at 51 evenly spaced points on the surface below the aircraft. Walsh et al. (1985) describe in detail the data processing used to produce directional wave spectra.

Figure 7 shows one of the SCR spectra obtained on 18 February 1986 during flight line 2. Each spectrum is an average of three nonoverlapping data segments approximately 5 km in the alongtrack direction. The spectrum is a polar plot in the wave number domain (2π/wavelength). The basic quantization in the spectrum is 10° by 0.01 m^{-1} and the spectral estimates in each bin have, in the worst case, 48 degrees of freedom at low wave numbers. The spectra are in terms of propagation vectors so that angles are referenced to the direction towards which the waves are propagating. The altitude of the NASA P-3 aircraft was ~450 m during flight lines 2 and 4 and the half-power footprint was $\sim 8 \times 11$ m. Under these circumstances, the SCR wave spectra should not be used for wavelengths $\leq$ 30 m (wave number $\geq$ 0.2 rad m^{-1}).

The spectrum shows both the real spectral components and the artifacts generated when the two-dimensional FFT is applied to the elevation data. The artifacts are identical to and rotated 180° from the lobes, since elevation data could represent waves propagating in either direction. Doppler corrections must be applied

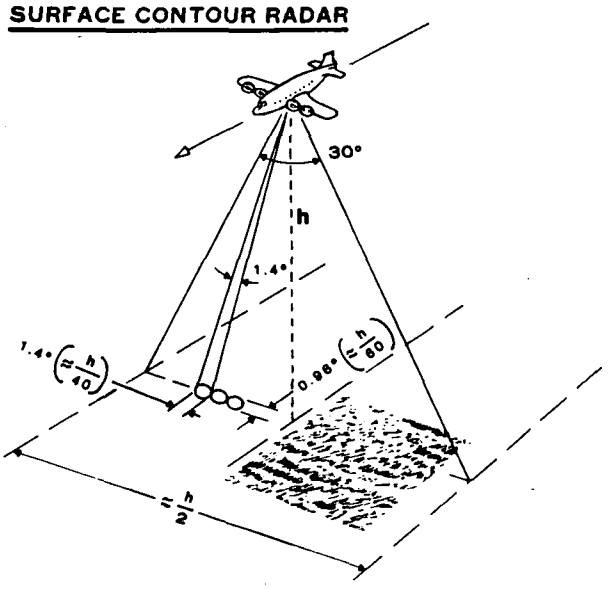

FIG. 6. A schematic diagram of the operation of the sea surface contour radar.

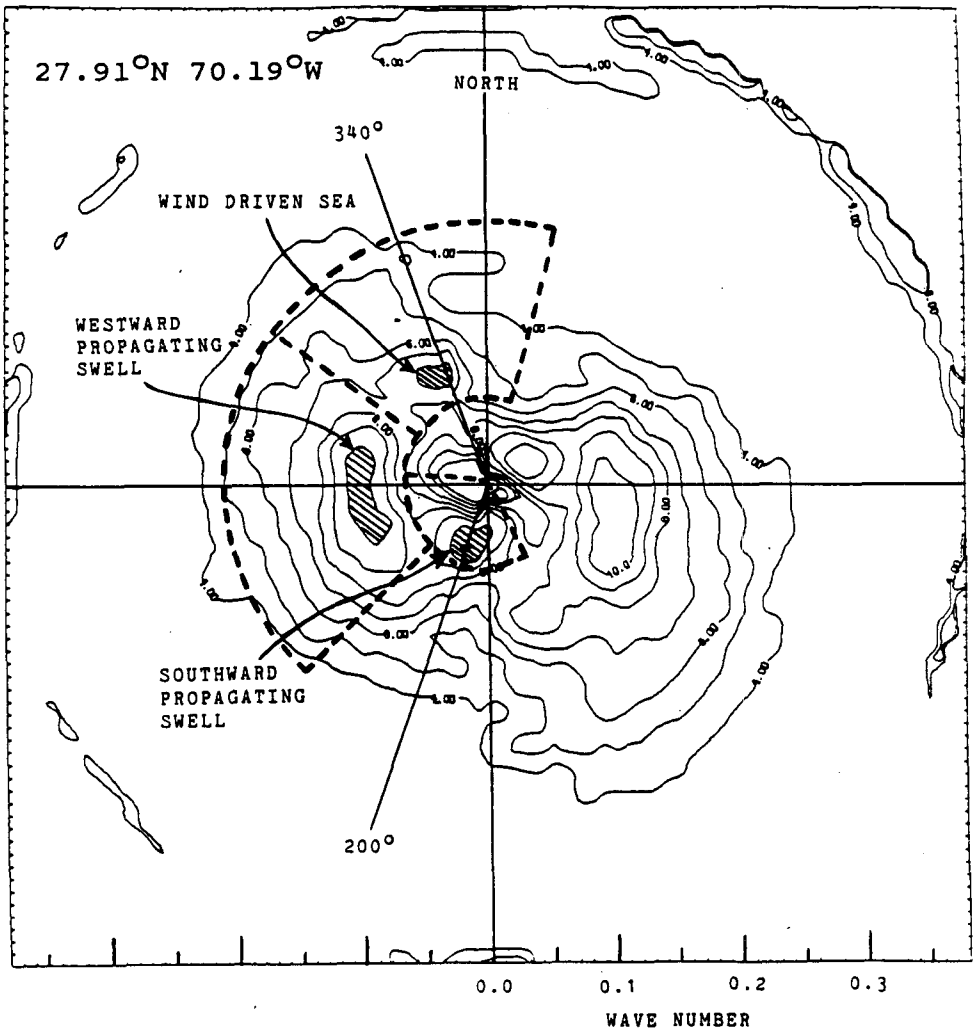

FIG. 7. The directional wave spectrum as observed by the SCR. Note the presence of the west- and southward propagating swell as well as the wind driven sea. The dash lines marked the regions of the spectrum used to evaluate the significant wave height for each of the wave components.

to compensate for the movement of the waves during the 50 s time interval it takes to record a data set used to obtain a spectrum. Once the Doppler corrections have been made, the artifacts are pushed out of their symmetrical positions by being shifted parallel to the aircraft alongtrack direction. This allows for their identification when spectra on different ground tracks are overlaid. The real spectral components will overlay while the artifacts will not.

From Fig. 7 the significant wave height (SWH, four times the surface height standard deviation) was estimated to be ~1.8 m and three wave systems were identified. One system had about a 60 m wavelength (6 s period, ~0.1 m^{-1} wavenumber) and propagated in the downwind direction (340°). The second system also had about a 60 m wavelength and propagated towards the west. The third system had about a 120 m wavelength (9 s period, 0.05 m^{-1} wavenumber) and propagated towards 190°.

In an attempt to quantify the behavior of the three wave components identified in Fig. 7, the variance within each of the three spectral regions outlined in Fig. 7 was computed for each of the spectra generated through the entire flight. The associated values of SWH for each component and their sum are plotted in Fig. 8 as a function of latitude and flight line number. Also shown are the frontal zone regions in the west (line 2) and the east (line 4). The most pronounced characteristic is that the total wave height was less north of the front. The south propagating swell appears to have increased in wave height when it encountered the front. The west propagating swell appears to have had a wave height maximum in the frontal zone. The wind-driven component appears to have decreased across the front.

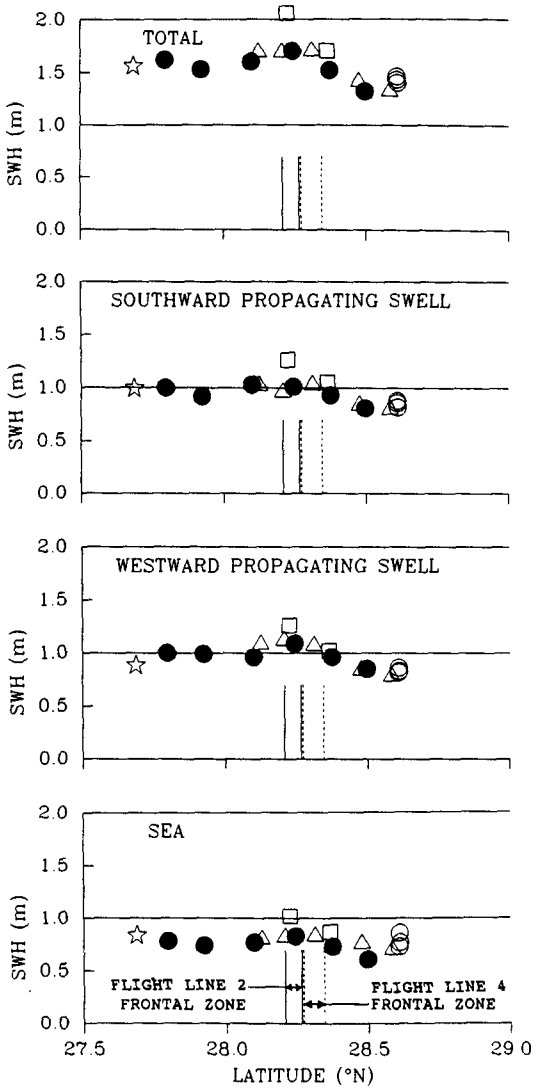

FIG. 8. A plot of the significant wave height (SWH) of the three wave components and the total sea vs. latitude. The solid circles indicate data taken on flight line 2. The open circles indicate data taken on flight lines 1 and 5. The star data point was taken on flight line 3. The squares and triangles were taken on flight line 4 and 6, respectively. Locations of the front are indicated. Note the slight decrease of the SWH on the north (cold) side of the front; the decrease was ~15%.

3. Data interpretation and discussion

The data described in section 2 present a unique situation to explore σ_0 variations with wind, wave, and atmospheric stratification.

TABLE 1a. σ_0 at downwind maxima, vertical polarization during flight line 2.

A	−15.4
B	−15.8
C	−15.9
D	−18.2

TABLE 1b. σ_0 at upwind maxima, horizontal polarization during flight line 4.

E	−19.9
F	−20.1
G	−19.7
H	−22.2

Downwind σ_0 maxima A, B and C (Fig. 2), and J, K, L, M and N (Fig. 4), and upwind σ_0 maxima E, F and G (Fig. 3) were selected to characterize σ_0 on the warm (southern) side of the front on flight lines 2, 6 and 4, respectively. The downwind maximum D (Fig. 2), and I (Fig. 4), and upwind maximum H (Fig. 3), characterize the cold (northern) side. Table 1 gives the σ_0 values determined for these maxima. During flight line 2 there was a warm (average of A, B and C) to cold (D) side differences of 2.5 dB. Similarly, the warm to cold side difference on lines 4 and 6 were 2.3 dB and 1.4 dB, respectively. The values of U (10 m), U_N (10 m), U_N (19.5 m) and u^* derived from ship and aircraft data are compiled in Table 2 for all three flight lines. For each flight line the Electra stress estimates centered south of 28.2°N (Fig. 4) were averaged to give the warm side Electra u^* values, because they spatially span the σ_0 maxima. There were no warm side ship u^* values available. The nearest *Oceanus* u^* was a 30-minute average centered an hour after the aircraft passed on flight line 2. Cold side u^* values from flight line 2 are the most northerly Electra u^* estimate and the coincidental 20-minute average u^* from Endeavor. From flight lines 4 and 6 the two most northerly Electra u^* estimates were average to give a cold side value, because they spanned the σ_0 maxima, H and I, respectively.

Spatial inhomogeneity precluded the use of σ_0 maxima and Electra stress estimates from the immediate vicinity of the front. Otherwise, the considerations for choosing the data for Table 2 were that ship u^* averages included the time of the overflights and that the Electra stress estimates spatially spanned the σ_0 maxima in the latitudinal direction. To ensure the latter, the C-130B latitudes were offset, so that they aligned with the Electra latitudes (Fig. 4) at the frontal crossing (the offsets of less than 0.05 degrees are well within the uncertainties of the INS data from the Electra and the C-130B). Also, the footprint of the σ_0 maxima was taken to be 1.2 km behind the C-130B, to account for flight and

TABLE 1c. σ_0 at downwind maxima, horizontal polarization, during flight line 6.

I	−3.2 dB
J	−1.7 dB
K	−1.9 dB
L	−1.6 dB
M	−1.7 dB
N	−1.9 dB

radar geometry (Fig. 1b). No attempt was made to adjust for a possible small misalignment in longitude, because Table 2 indicates that there was very little longitudinal change in wind variables. Similar selection criteria were used for the ship and Electra U, and hence U_N values in Table 2. The most difficult decisions were to exclude the most northerly and southerly downwind maxima from line 2 and the most southerly upwind maximum from line 4, but there was no Electra data corresponding to the footprint of any of these maxima. Figure 2 shows that these maxima would reduce both the warm and cold side σ_0 values of flight line 2, with little effect on the difference across the front.

In order to minimize the measurement uncertainties, the results from the ships and Electra were further averaged with weights applied in inverse proportion to their relative uncertainty. From Table 2a, we found from flight line 2 that the ratios of warm to cold side values of σ_0, U (10 m), U_N (10 m) U_N (19.5 m), and u^* were 1.78, 1.13, 1.16, 1.16 and 1.31, respectively. To facilitate comparisons, we adopt common practice and use a power law relationship between σ_0 and a wind variable, X, to express σ_0 as

$$\sigma_0 = K_1(X)^\alpha \tag{6}$$

or, if the logarithm is taken on both sides

TABLE 2. Comparison of σ_0 and various wind variables.

Parameter		Cold side value	Warm side value	Warm to cold ratio	α Mean	α Range
			(a) *Flight line 2*			
σ_0		−18.2 ± .05 dB	−15.7 ± .03 dB	1.78 ± 2%	—	
U (10 m)	Ship	8.2 ± 5%	9.2 ± 5%			
	Electra	7.6 ± 5%	8.8 ± 2.5%			
	Average	7.9 ± 3.5%	8.9 ± 2.2%	1.13 ± 4%	4.7	3.5–7.3
U_N (10 m)	Ship	8.0 ± 5%	9.2 ± 5%			
	Electra	7.3 ± 5%	8.8 ± 2.5%			
	Average	7.7 ± 3.5%	8.9 ± 2.2%	1.16 ± 4%	3.9	3.0–5.6
U_N (19.5 m)	Ship	8.5 ± 5%	9.8 ± 5%			
	Electra	7.8 ± 5%	9.4 ± 2.5%			
	Average	8.1 ± 3.5%	9.5 ± 2.2%	1.16 ± 4%	3.9	3.0–5.6
u^*	Ship	0.25 ± 15%				
	Electra	0.29 ± 30%	0.34 ± 13%			
	Average	0.26 ± 13%	0.34 ± 13%	1.31 ± 18%	2.1	1.3–8.3
			(b) *Flight line 4*			
σ_0		−22.2 ± .03 dB	−19.9 ± .03 dB	1.70 ± 2%		
U (10 m) (m s^{-1}) Electra		8.4 ± 5%	8.8 ± 2.5%	1.05 ± 6%	10.9	5.0–
U_N (10 m) (m s^{-1}) Electra		8.1 ± 5%	8.8 ± 2.5%	1.08 ± 6%	6.9	3.9–28
U_N (19.5 m) (m s^{-1}) Electra		8.6 ± 5%	9.3 ± 2.5%	1.08 ± 6%	6.9	3.9–28
u^* (m s^{-1}) Electra		.24 ± 21%	.31 ± 13%	1.30 ± 25%	2.0	1.06–
			(c) *Flight line 6*			
σ_0		−3.2 ± .05 dB	−1.76 ± .02 dB	1.82 ± 2%	—	
U (10 m) (m s^{-1}) Electra		7.37 ± 3.5%	8.61 ± 2%	1.17 ± 4%	3.0	1.6–2.1
U_N (10 m) (m s^{-1}) Electra		7.20 ± 3.5%	8.61 ± 2%	1.20 ± 4%	1.8	1.4–2.5
U_N (19.5 m) (m s^{-1}) Electra		7.57 ± 3.5%	9.06 ± 2%	1.20 ± 4%	1.8	1.4–2.5
u^* (m s^{-1}) Electra		.210 ± 21%	.316 ± 12%	1.50 ± 24%	0.8	0.5–2.6

$$\sigma_0\,(\mathrm{dB}) = 10\alpha \log X + K_2,$$

where K_1 and K_2 are arbitrary constants. The above ratios require that α has the values 4.7, 3.9, 3.9 and 2.1, respectively, to explain the U (10 m), U_N (10 m), U_N (19.5 m), and u^* cross-front variations.

The uncertainty in each ratio is used to compute an uncertainty range in which the actual value of α should fall. These uncertainty ranges shown in Table 2a are large, but still the observed results are inconsistent with the SASS-1 model (Schroeder et al. 1982), which reportedly relates σ_0 to U_N (19.5 m) as a power law. The SASS-1 exponent for vertical polarization at 50° incidence angle, downwind is 2.2, which is below the minimum of 3.0 indicated by the data, and well below the most likely value of 3.9. Our results using U (10 m) are even more inconsistent with previous studies (Moore and Fung 1979). In the study of Liu and Large (1981), the exponent for the σ_0 to u^* power law relationship at 40° angle of incidence, upwind, and vertical polarization was 2.3 (see their Table 2). Subsets of these data give an exponent of 2.4 for both 45 and 55° angles of incidence. Thus these results easily fall within the possible range of our observations and are near our most likely exponent value of 2.1.

The results shown in Figs. 3 and 4 indicate that similar conditions extended at least over the 60 km separation in longitude between flight lines 2 and 4. Table 2b shows that along flight line 4, the warm to cold side ratios of U (10 m), U_N (10 m) U_N (19.5 m) and u^* are 1.05, 1.08, 1.08 and 1.30, respectively, with corresponding values for α of 10.9, 6.9, 6.9, and 2.0. These values indicate that for horizontal polarization the SASS-I model also does not fit the data observed, but that the dependence on u^* appears to be consistent with SASS results of Liu and Large (1981).

The derived power law exponents for the four types of wind variables from flight line 6 are shown in Table 2c. The results presented, again, contradict with the SASS-I model, which shows a power law exponent of 0.9 at 20° incidence angle for horizontal polarization. This is well below the value derived for the U_N (19.5 m) case. The SASS-I model exponent value agrees more closely with that derived for the u^* case. However, as in the case with flight line 4, the uncertainty is quite large, due to the lack of ship observations. Nevertheless, the inconsistency of wind speed variations and the consistency of u^* changes does extend over the incidence angle range of 20 to 50 degrees, and from vertical to horizontal polarization.

The observed conditions at this SST front on 18 February 1986 likely reflect a complicated interaction between the wind, waves and currents. The southerly wind was observed to decrease as it crossed from the warm to cold side. Because the flow was from near neutral to quite stable stratification ($\zeta \approx 0.046$ at $z = 10$ m), there was a larger decrease in U_N. In addition there appears to have been a decrease in surface roughness, z_0, on the cold side that produced an even larger reduction in u^*. In other words, from (3), the neutral drag coefficient, and hence surface roughness were larger on the warm side than the cold side. This inferred z_0 change is in the same sense as the observed 15% difference in SWH (Fig. 7). Such behavior is expected, since the significant wave height is a measure of the wave height variance, and z_0 has sometimes been related to integrals of the wave height spectrum (Huang et al. 1986). The change in z_0 is not likely to be a consequence of the change in ζ, because $\psi(\zeta)$ is empirically formulated to make z_0 in (1) independent of stability. Furthermore, extensive direct measurements (Large 1979) do not show such a dependency.

The particular time of the flights does not appear to have been anomalous, because the structure of the atmospheric boundary layer along 70.3°W on 18 February 1986 seems to have persisted for at least eight hours. This picture is provided by the ships during their movements across the front. Oceanus steamed south along 70.3°W from 28.9°N, well on the cold side of the front, to its warm side meteorological station at 28.0°N, between 0800 and 1600 UTC. In so doing, it traversed the front about 1300 to 1430. Meanwhile Endeavor maintained oceanographic stations on the warm side of the front until about 1200, then moved north and then west to occupy its meteorological station at 28.5°N, where it remained from 1300 to 1630 UTC.

Both ships show a tendency for the neutral 10 m drag coefficient to be larger on the warm side of the front than the cold side. Since individual C_N values have a large uncertainty, as much averaging as possible was performed to see if this result was significant. Figure 9 shows data averaged up to two hours from the ships and aircraft as time series of C_N (10 m) on both sides of the front. Horizontal lines emanating from each point cover the averaging period while the vertical lines indicate the range of the individual values. The tendency for higher warm side values is clear and persistent. In total, there were 17 observations on the warm side, which gave an average 10^3 C_N (10 m) of 1.46 ± 0.20, where the uncertainty assumes independent observations. The 26 observations on the cold side gave an average of 1.02 ± 0.10 for 40% and 70% uncertainties in the ship and aircraft values, respectively. What emerges from these data is a temporally (from 0900 to 1700) and spatially (from 70.2° to 69.6°W) stable situation of a southerly wind blowing across a sharp SST front, and decreasing in speed (U_N) by 10–30%. This decrease is accompanied by a persistently greater decrease in u^* (20–60%), as reflected in the decrease in the drag coefficient (40–70%). We have also examined the σ_0 data taken during flight lines 1 and 3 (Fig. 1), and the results support this conclusion.

The result reported here can be used to illustrate difficulties of this type of σ_0 versus wind study if actual measurements of u^* are not directly performed. For example, a common approach in evaluating u^* is based

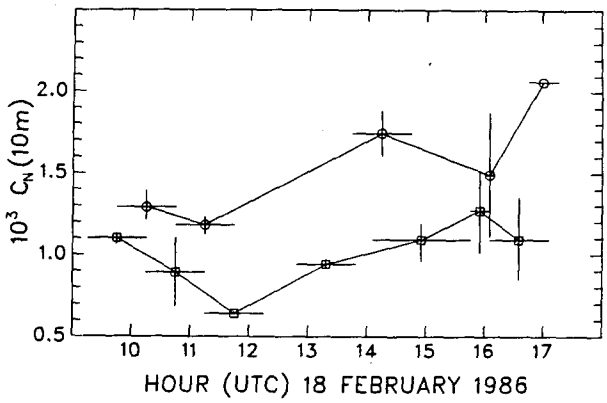

FIG. 9. Time series of C_{DN} (10 m) from both the warm (circles) and cold (squares) sides of the SST front. The averaging period and the range of the individual observations are shown by the horizontal and vertical lines, respectively.

on the bulk formulation. If one only obtains the U_N (10 m) measurements and proceeds to use the ensemble averaged value of the neutral drag coefficient (e.g., the formula shown in Large and Pond 1981), one would necessarily infer that the u^* variation across the front was the same as the U_N (10 m) variation, since the ensemble averaged neutral drag coefficient was the same [Eq. (3)]. The exponent required for the inferred u^* would be the same as that of U_N (10 m). Since this exponent is high compared to the results reported previously, one may draw the (wrong) conclusion that there must be another major contributor to σ_0 variation. An obvious candidate for this variable is the sea state since the SWH varied across the front. One can imagine an erroneous model function constructed on this argument and the lack of actual u^* measurements.

Of course, with the limited data presented here, we cannot rule out that the sea state changes also contributed directly to the variations in σ_0 say, through the mean slope changes. In fact, a recent model by Plant (1986) contains an explicit dependence of the radar backscatter cross section on the mean wave slope. For certain situations, his model indicates that σ_0 can change substantially as the wave slope varies for constant near surface wind (e.g. see Fig. 11 in Plant 1986). This behavior is qualitatively similar to the data shown in Keller et al. (1985). However, the results in Keller et al. cannot be directly interpreted because of the lack of actual u^* measurements, as shown above. Again, modifications of the drag coefficient due to long-wave slope changes might have accounted for some of the variations observed. At present, it is difficult to apply the Plant model to our observed wave spectrum data because the model cannot be easily extended to oceans with significant swells propagating at angles offset from the wind. Furthermore, it is not clear that the wavenumbers with significant contribution to the mean wave slope, as defined by Plant, were even measured with the SCR. From our observed results, however, we speculate that the prime role the sea state variations played was to modify the roughness length (z_0) and hence the observed drag coefficients (e.g. see Huang et al. 1986; Kahma 1987). Since our observed σ_0 changes can be entirely explained by the u^* changes (within the measurement uncertainties, and using the Liu and Large results) we cannot measure any direct effects of sea state variations. A more promising approach to evaluate the effects of wave spectrum and spectrum change on σ_0 is to examine the azimuthal variations of σ_0. For example, we can evaluate the detailed azimuthal variations in the directions of the south and west propagation swells and determine if there is any asymmetry that can be explained on this basis. It would be interesting to modify Plant's model for these swell conditions and evaluate whether the predictions are consistent with the observed azimuthal variations.

Another interesting feature in the σ_0 variations across the SST shown in Fig. 2 is the gradual nature of the σ_0 decrease on the cold (downwind) side of the front. We estimate that the spatial scale over which the σ_0 transition was completed was 10 km. This distance might be an important input to air–sea interaction models for the frontal structure.

A recent theoretical model of Donelan and Pierson (1987) contrasts with power law models such as SASS-I. This model cannot be rigorously tested with our data, because it does not specifically treat situations with three component wave system shown in Fig. 6 and the presence of an oceanic front. Nonetheless, there are some features worth noting. Donelan and Pierson choose to formulate their model in terms of $U(\lambda/2)$, where λ is the wavelength of the backscattering elements, rather than in terms of either u^* or U (19.5 m). Changes in $U(\lambda/2)$ across the SST front would be even smaller than those in U(19.5 m). At the wind speeds of this case study the Donelan-Pierson model is not much different than SASS-I, and for flight line 2 it predicts only about a 1.1 dB change in downwind σ_0 across the front.

The results presented here represent one particular open ocean situation. They suggest the existence of a universal σ_0 to u^* relationship, but it could be fortuitous. They do, however, show that the SASS-I model did not hold in these particular conditions. Many more case studies of this kind are required in order to assess the significance of this kind of behavior on global wind retrievals from satellite scatterometers.

There have recently been suggestions that in computing wind stress from mean winds, the drag coefficient should be adjusted according to wind and wave conditions (e.g. Large and Pond 1981: Geernaert et al. 1987). Our study indicates that such adjustments should not be applied when the winds are derived from microwave backscatter because the backscatter itself may be modulated in the proper sense by the wind and wave conditions. That is, when the local drag coefficient is higher than average, the backscatter appears to in-

crease following the stress, and the derived winds are erroneously high. Therefore, use of an average drag coefficient is appropriate for calculating the most accurate stress.

Acknowledgments. The research described in this paper by F. Li was performed by the Jet Propulsion Laboratory, California Institute of Technology, under contract with the National Aeronautics and Space Administration. The participation of AMSCAT and the Surface Contour Radar in FASINEX was made possible by the supporting research and technology program of the NASA Oceanic Processes Branch. We thank Drs. W. Patzert and S. Wilson for their support. W. G. Large was supported by the National Aeronautics and Space Administration (Grant NASA-W-15, 969), by the U.S. Office of Naval Research (Contract N001114-85-F-031), and by the National Science Foundation through its sponsorship of the National Center for Atmospheric Research. W. Shaw was supported by the National Science Foundation with Grant OCE-8603050.

Note added in proof. Since the NCAR Electra was flying at an altitude of 40 m, we expected that the measured stress would vary negligibly between flight level and the surface. On 18 February, the NRL P-3A was also flying in formation at an intermediate altitude of 100 m. Preliminary stress measurements from the NRL P-3A (Friehe, private communication) indicated that there was a small variation of stress with altitude on the warm side of the front as compared with the Electra results but a considerable variation on the cold side. Extrapolation of these results to the surface would lead to a smaller change in the surface stress across the front than that indicated in our Table 2. However, because of the good agreement between the Electra and the ship measurements (Fig. 5) and the consistent change of the drag coefficient across the front (Fig. 9) as indicated by the ship measurements, this possible variation was not taken into account in the present analysis.

REFERENCES

Donelan, M. A., and W. J. Pierson, Jr., 1987: Radar scattering and equilibrium ranges in wind-generated waves with application to scatterometry. *J. Geophys. Res.*, **92**C5, 4971–5029.

Geernaert, G. L., S. E. Larson and F. Hansen, 1987: Measurements of the wind stress, heat flux and turbulence intensity during storm conditions over the North Sea. *J. Geophys. Res.*, **92**, 13127–13139.

Guest, P. S., and K. L. Davidson, 1987: The effect of observed ice conditions on the drag coefficient in the summer east Greenland sea marginal ice zone. *J. Geophys. Res.*, **92**, 6943–6954.

Halberstam, J., 1980: Some considerations in the evaluation of SEASAT-A Scatterometer (SASS) measurements. *J. Phys. Oceanogr.*, **10**, 623–632.

Huang, N. E., L. F. Bliven, S. R. Long and P. S. De Leonibus, 1986: A study of the relationship among wind speed, sea state, and the Drag Coefficient for a developing wave field. *J. Geophys. Res.*, **91**(C6), 7733–7742.

Jones, W. L., L. C. Schroeder and J. L. Mitchell, 1977: Aircraft measurements of the microwave scattering signature of the ocean. *IEEE J. Oceanic Eng.*, **OE-2**, 52.

Kahma, K. K., 1987: Calculation of the Drag Coefficient over waves by means of the wave spectrum.

Kaimal, J. C., J. C. Wyngaard, Y. Izumi and O. R. Cote, 1972: Spectral characteristics of surface-layer turbulence. *Quart. J. Roy. Meteor. Soc.*, **98**, 563–589.

Keller, W. C., W. J. Plant and D. E. Weissman, 1985: The dependence of X-band microwave sea return on atmospheric stability and sea state. *J. Geophys. Res.*, **90**, 1019–1029.

Kenny, J. E., E. A. Uliana and E. J. Walsh, 1979: The surface contour radar; a unique remote sensing instrument. *IEEE Trans. Microwave Theory Tech.*, MTT **2712**, 1080–1092.

Large, W. G., 1979: The turbulent fluxes of momentum and sensible heat over the open sea during moderate to strong winds. Ph.D. thesis, University of British Columbia, 180 pp.

——, and S. Pond, 1981: Open-ocean momentum flux measurements in moderate to strong winds. *J. Phys. Oceanogr.*, **11**, 324–336.

——, and ——, 1982: Sensible and latent heat flux measurements over the ocean. *J. Phys. Oceanogr.*, **12**, 464–482.

——, and J. A. Businger, 1988: A system for remote measurements of the wind stress over the ocean. *J. Atmos. Oceanic Technol.*, **5**, 274–285.

Lenschow, D. H., and B. D. Stankov, 1986: Length scales in the convective boundary layer. *J. Atmos. Sci.*, **43**, 1198–1209.

——, and P. Spyers-Duran, 1987: Measurement techniques: Air motion sensing. NCAR RAF Bulletin 23, The National Center for Atmospheric Research, 49 pp.

Li, F., P. Callahan, D. Lame and C. Winn, 1984: NASA Scatterometer on NROSS—A system for global observations of oceanic winds. *Proc. IGARSS*, Strasbourg, France.

Liu, W. T., and W. G. Large, 1981: Determination of surface stress by Seasat-SASS: A case study with JASIN data. *J. Phys. Oceanogr.*, **12**, 1603–1611.

Monin, A. S., and A. M. Yaglom, 1965, 1967: *Statistical Fluid Dynamics, Vols. I and II.* English Translation, J. L. Lumby, Ed., MIT Press, 639 pp., 720 pp.

Moore, R. K., and A. K. Fung, 1979: Radar determination of winds at sea. *Proc. IEEE*, **67**, 1504–1521.

Plant, W. J., 1986: A Two-scale model of short wind-generated waves and scatterometry. *J. Geophys. Res.*, **91**(C9), 10735–10749.

Schroeder, L. C., D. H. Boggs, G. J. Dome, I. M. Halberstam, W. L. Jones, W. J. Piereson and F. W. Wentz, 1982: The relationship between wind vector and normalized radar crossection used to derived Seasat-A satellite scatterometer winds. *J. Geophys. Res.*, **87**, 3318–3336.

Scott, 1985: Directional wave spectra measured with the surface contour radar. *J. Phys. Oceanogr.*, **15**, 566–592.

Stage, S. A., and R. A. Weller, 1985: The frontal experiment (FASINEX), Part I: Background and scientific objectives. *Bull. Amer. Meteor. Soc.*, **66**, 1511–1520.

Walsh, E. J., D. W. Hancock III, D. E. Hines, R. N. Swift and J. F. Scott, 1985: Directional wave spectra measured with the Surface Contour Radar. *J. Phys. Oceanogr.*, **15**(5), 566–591.

Woiceshyn, P. M., M. G. Wurtele, D. H. Boggs, L. F. McGroblrick and S. Peteherych, 1986: The necessity for a new parametrization of an empirical model for wind/ocean scatterometry. *J. Geophys. Res.*, **91**, 2273–2289.

Wyngaard, J. C., 1973: On surface-layer turbulence. *Workshop on Micrometeorology*, D. A. Haugen, Ed., Amer. Meteor. Soc., Boston, 101–149.

——, 1985: Measurement physics. *Probing the Atmospheric Boundary Layer.* D. Lenschow, Ed., Amer. Meteor. Soc.